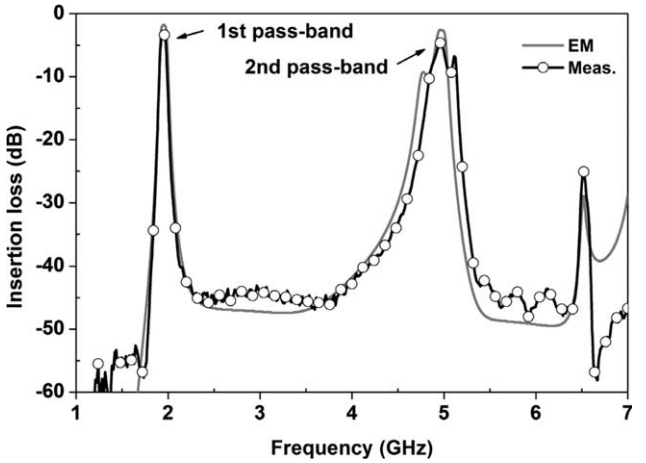

Figure 6 Comparison of simulated and measured second passbands

losses are assumed to be attributable to not applying a housing to the measurement.

Figure 6 shows the frequency responses of the simulated and measured second passbands, which nearly coincide at 4.96 GHz. Although showing some differences in the losses of the passband, the simulated and measured results have very good agreement and trend.

5. CONCLUSION

A novel SIR that can form the second passband further away compared to the conventional SIR is proposed. In case of its application to the coupled line BPF, the length of the coupled line constituting the SIR can be extended intentionally, which is very effective in implementing the gap of the coupled line having tight coupling. In addition, design formulas of the coupled line BPF applying the proposed SIR are derived. The theoretical validity is proven by the proposed SIR BPF design based on the presented formulas, simulation, fabrication, and measurement.

REFERENCES

1. M. Makimoto and S. SadaHiko, Bandpass filter using parallel coupled stripline stepped impedance resonator, IEEE Trans Microwave Theory Tech 28 (1980), 1413–1417.
2. M. Sagawa, M. Makimoto, and S. Yamashita, A design method of bandpass filter coaxial resonator, IEEE Trans Microwave Theory Tech 33 (1985), 152–157.
3. S. Yamashita and M. Makimoto, Miniaturized coaxial resonator partially loaded with high-dielectric-constant microwave ceramics, IEEE Trans Microwave Theory Tech 31 (1983), 697–703.
4. M. Sagawa, M. Makimoto, and S. Yamashita, Geometrical structures and fundamental characteristics of microwave stepped-impedance resonator, IEEE Trans Microwave Theory Tech 45 (1997), 1078–1085.
5. M. Makimoto and S. Yamashita, Microwave resonators and filters for wireless communication theory, design and application, Springer, Berlin, Germany, 2001, pp. 65–84.
6. G. Matthaei, L. Young, and E.M.T. Jones, Microwave filters, impedance-matching networks, and couplings structures, Artech House, Norwood, MA, 1980.
7. S.B. Cohn, Parallel coupled transmission-line resonator filters, IRE Trans Microwave Theory Tech 6 (1958), 223–231.

COMBINED-TYPE TRIPLE-WIDEBAND LTE TABLET COMPUTER ANTENNA

Kin-Lu Wong and Chih-Yu Tsai
Department of Electrical Engineering, National Sun Yat-sen University, Kaohsiung 80424, Taiwan; Corresponding author: wongkl@ema.ee.nsysu.edu.tw

Received 26 September 2014

ABSTRACT: *A combined-type triple-wideband tablet computer antenna covering the long term evolution (LTE) operation in the 698–960 MHz (low band), 1710–2690 MHz (middle band), and 3400–3800 MHz (high band) is presented. The antenna is formed by an inverted-F antenna (IFA) covering the LTE low band and a coupled-fed loop antenna covering the LTE middle and high bands. The IFA (low-band antenna) and coupled-fed loop antenna (middle/high-band antenna) are easily combined into a compact structure to occupy a small ground clearance of 10 × 30 mm^2 and a thin thickness of 3 mm. Details of the antenna structure are described in this study. Working principle of the antenna to achieve the LTE triple-wideband operation through combining the low-band antenna and the middle/high-band antenna is addressed. Experimental results of the fabricated antenna are also presented and discussed.* © 2015 Wiley Periodicals, Inc. Microwave Opt Technol Lett 57:1262–1267, 2015; View this article online at wileyonlinelibrary.com. DOI 10.1002/mop.29066

Key words: *mobile antennas; tablet computer antennas; LTE antennas; combined-type antennas; triple-wideband antennas; small-size antennas*

1. INTRODUCTION

The combined-type antenna [1,2] has recently been shown to be a promising antenna design to achieve the long term evolution (LTE) dual-wideband operation in the 698–960 and 1710–2690 MHz bands with a small antenna size [3]. The combined-type antenna is easily and conveniently formed by combining a low-wideband antenna and a high-wideband antenna into a compact structure. The low-wideband antenna covers the 698–960 MHz band while the high-wideband antenna covers the 1710–2690 MHz band. The low and high widebands are covered by separate antenna elements, making it easy in achieving dual-wideband operation. In addition, it has been shown that the required ground clearance for the combined-type dual-wideband antenna is as small as 10 × 30 mm^2 and the thickness there of is 3 mm only for the tablet computer application [2]. As the occupied ground clearance of 10 × 30 mm^2 is small compared to many recently reported LTE tablet computer antennas [4–15], the combined-type antenna is attractive for practical LTE applications.

In this article, we demonstrate a triple-wideband combined-type antenna to cover the LTE operation in the 698–960 MHz (low band), 1710–2690 MHz (middle band), and 3400–3800 MHz (high band) [3,16,17]. The high band of 3400–3800 MHz is a new LTE band allocated recently [3]. The proposed antenna covers the complete LTE triple-wideband operation with a small antenna size of 10 × 30 × 3 mm^3 for the tablet computer application. The occupied size of the proposed antenna is the same as that in [2] for the combined-type dual-wideband antenna but with an additional LTE high-band coverage.

The antenna is formed by combining an inverted-F antenna (IFA) covering the LTE low band and a coupled-fed loop antenna covering the LTE middle and high bands. The antenna structure is described in detail in this study, and working principle of the antenna to achieve the LTE triple-wideband operation is addressed. The antenna is also fabricated, and the experimental results are presented and discussed.

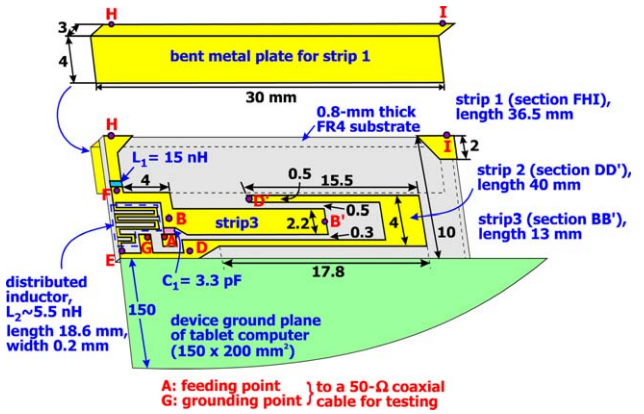

Figure 1 Geometry of the combined-type triple-wideband LTE tablet computer antenna. [Color figure can be viewed in the online issue, which is available at wileyonlinelibrary.com]

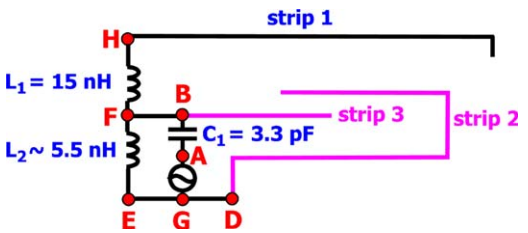

Figure 2 Simplified structure for the antenna with circuit elements embedded therein. [Color figure can be viewed in the online issue, which is available at wileyonlinelibrary.com]

2. PROPOSED ANTENNA

2.1. Antenna Structure

Figure 1 shows the geometry of the combined-type triple-wideband LTE tablet computer antenna. The total antenna volume is $10 \times 30 \times 3$ mm^3, and the antenna is mounted along the top edge of the device ground plane with dimensions of 200 mm in length and 150 mm in width. The ground plane dimensions are selected to fit for a 9.7-in. tablet computer. To show the antenna structure more clearly for understanding, Figure 2 shows a simplified structure of the antenna with circuit elements embedded therein. The antenna is obtained by combining a low-band antenna and a middle/high-band antenna. The low-band antenna is an IFA for covering the 698–960 MHz band [see the antenna structure of Ant1 in Fig. 3(a)]. The middle/high-band antenna is a coupled-fed loop antenna for covering the 1710–2690/3400–3800 MHz bands [see the antenna structure of Ant2 in Fig. 3(b)]. Corresponding simplified structures of Ant1 and Ant2 are also shown in Figure 3 for comparison. The two antennas share a short-feeding strip (section AB) with a chip capacitor (C_1) of 3.3 pF embedded therein. The capacitor C_1 is added for bandwidth enhancement of Ant1, and it generally does not affect the achievable bandwidth of Ant2 because it contributes low-capacitive reactance ($1/j\omega C$) at frequencies in the LTE middle and high bands.

To have a small antenna size and a wide operating band for Ant1 to cover the LTE low band, a bent metal plate for the IFA's main radiating arm (strip 1) is connected to the feeding strip (section AB) and shorting strip (section EF) through a chip inductor (L_1) of 15 nH. The bent metal plate provides a wider width for strip 1 to have an achievable wider bandwidth for Ant1. In the experimental study, the bent metal plate is cut from a 0.2-mm thick copper plate. Other portions of the antenna are printed on an FR4 substrate of thickness 0.8 mm, relative permittivity 4.4, and loss tangent 0.024. In the shorting strip, a distributed inductor (L_2) is embedded [18,19], which combines with the capacitor C_1 in the feeding strip to form a high-pass matching circuit to widen the bandwidth of Ant1. As the inductor L_2 requires a relatively small inductance of about 5.5 nH, it is formed in this study by printing a long narrow strip of length 18.6 mm and width 0.2 mm on the FR4 substrate. This simplifies the fabrication of the antenna. Also, note that a short strip (section BF) is used to connect the feeding strip and shorting strip, so that the distributed inductor L_2 can be accommodated

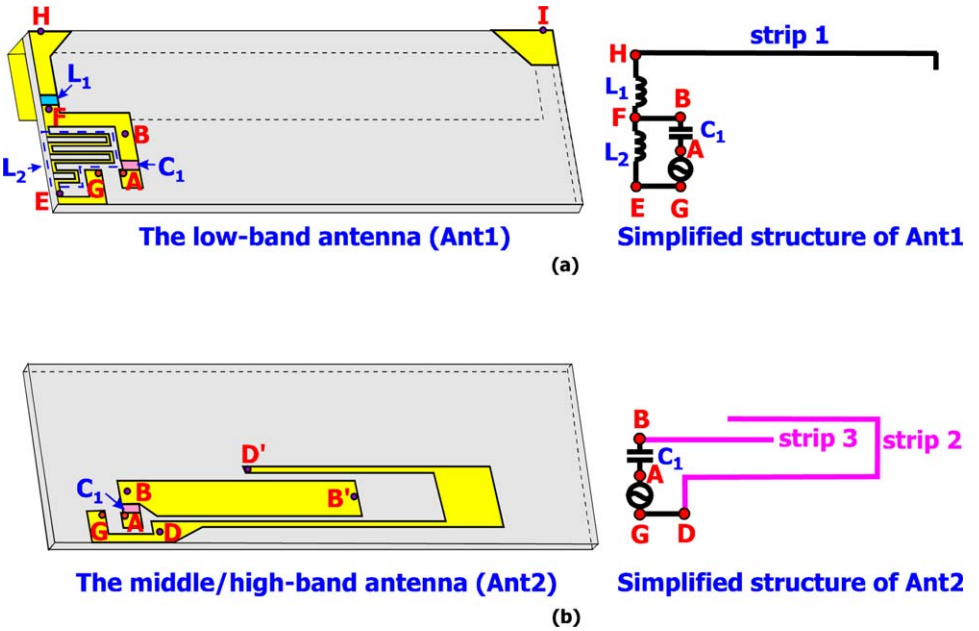

Figure 3 (a) The low-band antenna (Ant1). (b) The middle/high-band antenna (Ant2). [Color figure can be viewed in the online issue, which is available at wileyonlinelibrary.com]

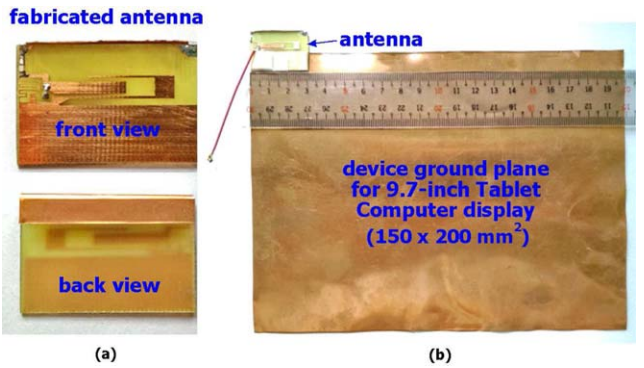

Figure 4 Photos of (a) the fabricated antenna and (b) the same mounted at the top edge of the device ground plane for experimental testing. [Color figure can be viewed in the online issue, which is available at wileyonlinelibrary.com]

in the space between section AB and EF. In this case, the short strip of section BF can also contribute to provide a longer radiating arm for Ant1.

Ant2 comprises two main radiating sections of strip 2 (section DD′) and strip 3 (section BB′). Strip 2 has a length of 40 mm, which is capacitively excited by strip 3 with a length of 13 mm. Strips 2 and 3 are formed as a coupled-fed loop antenna [20–22], which can provide a very wide operating band in this study to cover the LTE middle and high bands. To feed the antenna in the experimental testing, a 50-Ω coaxial line is applied (see the antenna photos shown in Fig. 4). The central conductor and outer grounding sheath of the coaxial line are connected, respectively, to point A (the feeding point) and G (the grounding point). In the experiment, the antenna is flushed to one corner of the top edge of the device ground plane. The experimental results will be presented in Section 3.

2.2. *Working Principle*

The simulated results obtained using the full-wave electromagnetic field simulator HFSS version 15 [23] are presented to analyze the working principle of the proposed antenna. Figure 5 shows the simulated return loss for the proposed antenna, Ant1, and Ant2. It is clearly seen that Ant1 (an IFA as the low-band antenna) has a wide operating band, that is, promising to cover the LTE low band, with no operating bands excited at higher frequencies. Conversely, Ant2 (a coupled-fed loop antenna as the middle/high-band antenna) provides a very wide operating

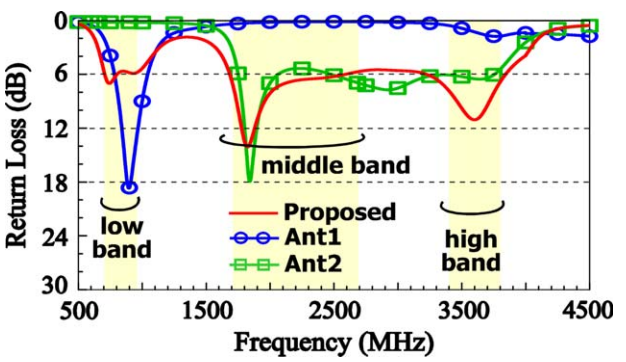

Figure 5 Simulated return loss for the proposed antenna, Ant1, and Ant2. [Color figure can be viewed in the online issue, which is available at wileyonlinelibrary.com]

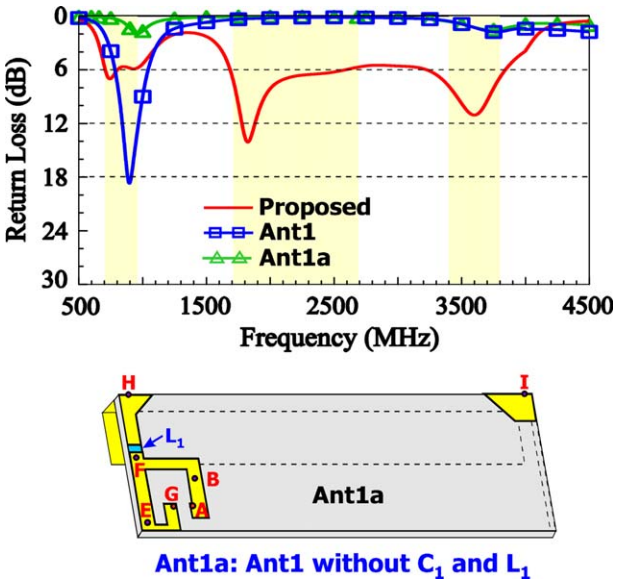

Figure 6 Simulated return loss for Ant1 without C_1 and L_2 (Ant1a), Ant1, and proposed antenna. [Color figure can be viewed in the online issue, which is available at wileyonlinelibrary.com]

band and is promising to cover the LTE middle and high bands. Ant2 also provides no operating bands at lower frequencies. The proposed antenna, which is obtained by combining Ant1 and Ant2, covers the LTE triple-wideband operation (698–960/1710–2690/3400–3800 MHz).

To analyze the working principle of Ant1, Figure 6 shows the simulated return loss for Ant1 without C_1 and L_2 (Ant1a), Ant1, and proposed antenna. The corresponding results of the simulated input impedance on the Smith chart for Ant1a (curve 1), Ant1 (curve 2), and proposed antenna (curve 3) in the low band of 650–1000 MHz are shown in Figure 7. For Ant1a, which is an IFA with a simple feeding strip and shorting strip, a resonant mode is excited in the LTE low band, although the IFA's radiating arm (strip 1) has a length (36.5 mm, about 0.11-wavelength at 900 MHz) much shorter than 0.25-wavelength at 900 MHz. This behavior is mainly owing to the embedded

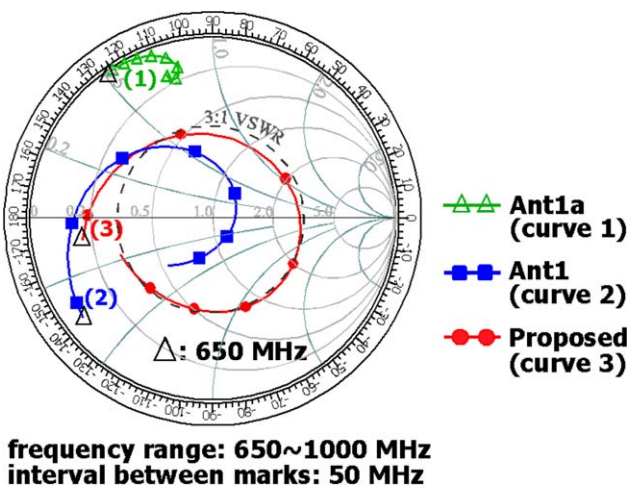

Figure 7 Simulated input impedance on the Smith chart for Ant1a (curve 1), Ant1 (curve 2), and proposed antenna (curve 3) in the low band of 650–1000 MHz. [Color figure can be viewed in the online issue, which is available at wileyonlinelibrary.com]

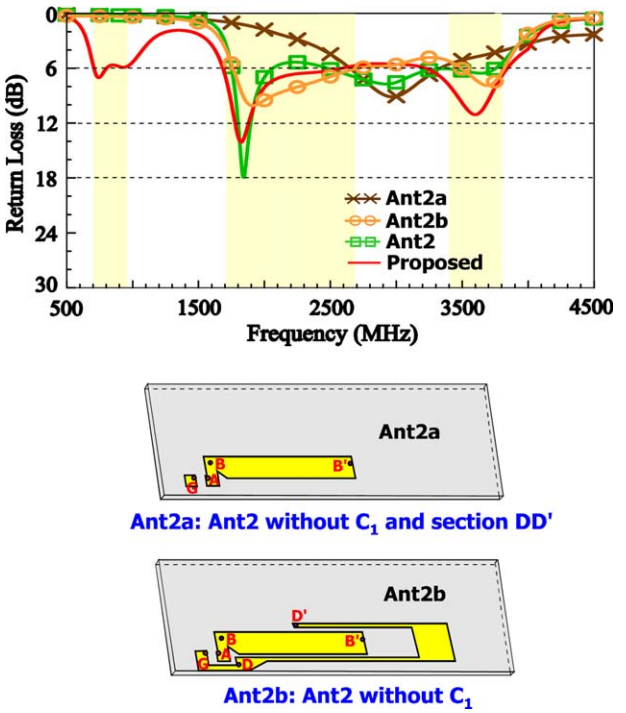

Figure 8 Simulated return loss for Ant2 without C_1 and section DD′ (Ant2a), Ant2 without C_1 (Ant2b), Ant2, and proposed antenna. [Color figure can be viewed in the online issue, which is available at wileyonlinelibrary.com]

inductor L_1, which decreases the required resonant length of the IFA's fundamental mode. However, the impedance matching of the excited resonant mode at about 900 MHz is very poor. From the input impedance shown in Figure 7, both the real and imaginary parts of the input impedance for Ant1 (see curve 1 in the figure) are very small, compared to 50 Ω, which causes poor impedance matching. When L_2 and C_1 are, respectively, embedded in the shorting strip and feeding strip, an embedded high-pass matching circuit is obtained, which leads to good impedance matching of the excited resonant mode. As shown in Figure 6, a wide bandwidth, that is, promising to cover the LTE low band is obtained for Ant1. From the input impedance shown in Figure 7, it is also clearly seen that a large part of the input impedance curve is shifted into the 3:1 VSWR circle (see curve 2 vs. curve 1 in the figure). Then, with Ant2 added to Ant1 to form the proposed antenna (see the results in Figs. 6 and 7), the antenna can provide a wide operating band to cover the desired LTE low band. As Ant1 dominates the coverage of the LTE low band, Ant1 is denoted as the low-band antenna in the proposed design.

Working principle of Ant2 to cover the LTE middle and high bands is analyzed with the aid of Figures 8 and 9. Results of the simulated return loss for Ant2 without C_1 and section DD′ (Ant2a), Ant2 without C_1 (Ant2b), Ant2, and proposed antenna are shown in Figure 8. The corresponding results of the input impedance of Ant2a and Ant2b are shown in Figure 9(a), and those for Ant2 and proposed antenna are shown in Figure 9(b). For Ant2a, which is a simple monopole antenna, a resonant mode is generated at about 3.0 GHz. By adding section DD′ to Ant2a (i.e., Ant2b is formed), a coupled-fed loop antenna can be obtained [20–22]. Additional resonant modes can occur at about 2.0 and 3.7 GHz, which are, respectively, the 0.25-wavelength and 0.5-wavelength loop modes [24,25], and a very wide operating band of about 2.1 GHz (from about 1.7 to 3.8 GHz), that is, promising to cover the LTE middle and high bands is obtained. From the results of curve 2 for Ant2b versus curve 1 for Ant2a shown in Figure 9(a), it is seen that curve 2 becomes a double-looped curve, indicating that multiple resonant modes are generated for Ant2b. A much wider operating band can be obtained for Ant2b.

With the presence of C_1 in section AB of Ant2b, Ant2 is formed. As the capacitor C_1 (3.3 pF used in this study) contributes small capacitive reactance at higher frequencies, it causes small variations on the impedance matching (see Ant2 vs. Ant2b in Fig. 8). Similarly, by adding Ant1 to form the proposed antenna, small variations on the impedance matching for frequencies in the LTE middle and high bands are also seen. Both curve 3 for Ant2 and curve 4 for the proposed antenna still have a double-looped characteristic as seen in Figure 9(b). The results indicate that the very wide operating band of about 1.7–3.8 GHz obtained for the proposed antenna to cover the desired LTE middle and high bands is mainly owing to Ant2. Ant2 is hence denoted as the middle/high-band antenna in the proposed design.

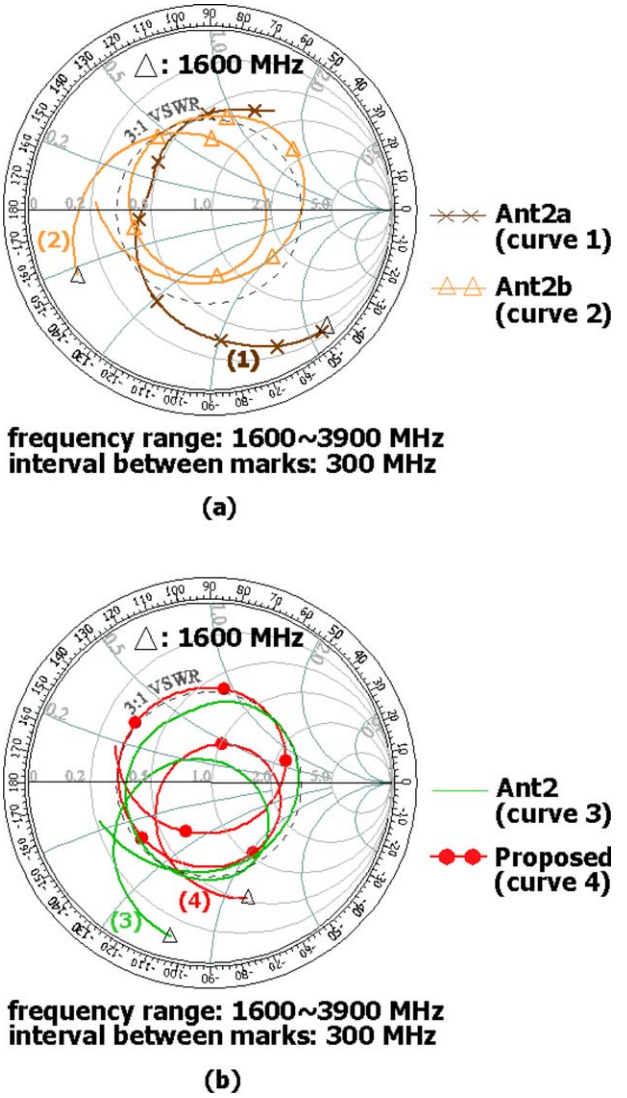

Figure 9 Simulated input impedance on the Smith chart for the middle and high bands of 1600–3900 MHz. (a) Ant2a (curve 1) and Ant2b (curve 2). (b) Ant2 (curve 3) and proposed antenna (curve 4). [Color figure can be viewed in the online issue, which is available at wileyonlinelibrary.com]

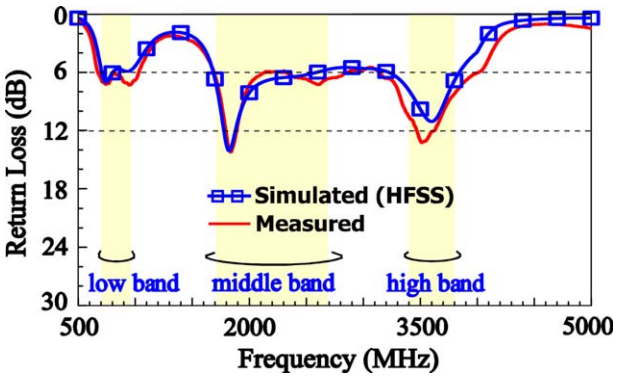

Figure 10 Measured and simulated return losses of the fabricated antenna. [Color figure can be viewed in the online issue, which is available at wileyonlinelibrary.com]

3. EXPERIMENTAL RESULTS

The proposed antenna was fabricated as shown in Figure 4. The measured and simulated return losses of the fabricated antenna are shown in Figure 10. The measured data agree with the simulated results. From the measured data, the proposed antenna can cover the LTE low, middle, and high bands with impedance matching better than 6-dB return loss (3:1 VSWR). The measured and simulated antenna efficiencies of the fabricated antenna are presented in Figure 11. The radiation characteristics are measured in a far-field anechoic chamber, and the antenna efficiencies include the mismatching losses. The measured efficiencies also generally agree with the simulated efficiencies. From the measured results, the antenna efficiencies are about 40–58% for the LTE low band, 60–78% for the LTE middle band, and 70–83% for the LTE high band. The obtained antenna efficiencies are acceptable for practical mobile communication applications [16,17].

The measured radiation patterns of the fabricated antenna at 850, 2500, and 3600 MHz are plotted in Figure 12. Simulated radiation patterns are also presented for comparison. Agreement between the measurement and simulation is also seen. At each frequency, the radiation intensities in the three principal planes are normalized with respect to the same maximum intensity. At 850 MHz (a representative frequency in the LTE low band), the E_θ radiation in the x-y plane (azimuthal plane) is smoothly varied in various ϕ directions and is close to near-omnidirectional. While those in the x-y plane seen at 2500 MHz (a representative

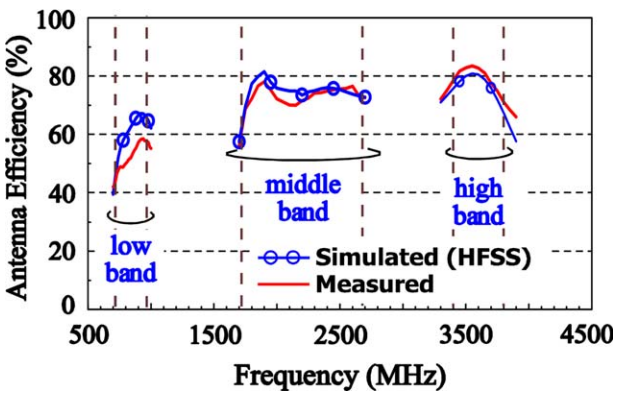

Figure 11 Measured and simulated antenna efficiencies of the fabricated antenna. [Color figure can be viewed in the online issue, which is available at wileyonlinelibrary.com]

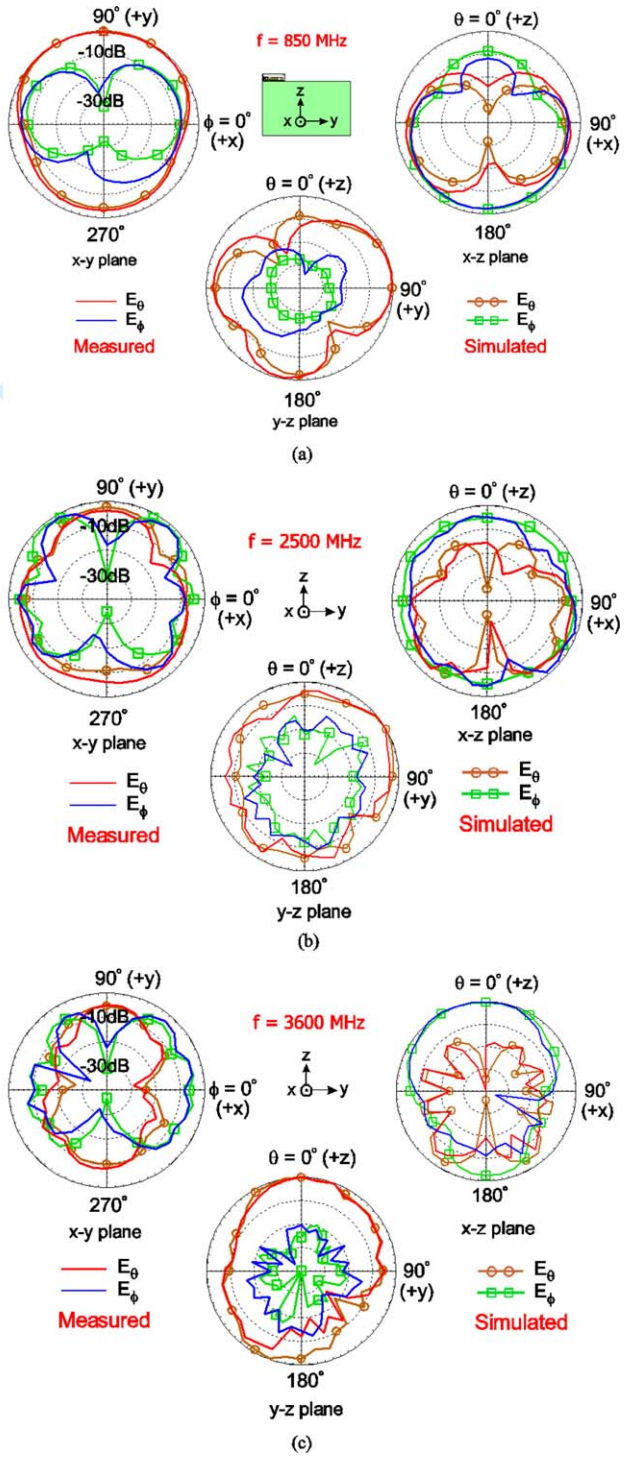

Figure 12 Measured radiation patterns of the fabricated antenna. [Color figure can be viewed in the online issue, which is available at wileyonlinelibrary.com]

frequency in the LTE middle band) and at 3600 MHz (a representative frequency in the LTE high band) show large variations in various ϕ directions. The different observations are owing to the wavelength at 850 MHz being much larger than that at 2500 and 3600 MHz.

In the y-z plane (elevation plane parallel to the device ground plane), asymmetric radiation patterns for the three frequencies are seen. This is because the antenna is mounted asymmetrically along the top edge of the device ground plane. In the x-z plane

(elevation plane vertical to the device ground plane), strong radiation in the lower half-plane ($-z$ direction) is observed at 850 MHz. However, strong radiation in the upper half-plane ($+z$ direction) is seen at 3600 MHz. This behavior is largely because the device ground plane contributes strongly to the radiation at 850 MHz and, on the contrary, acts more like a reflector at 3600 MHz. The observed radiation characteristics are similar to those of the reported LTE tablet computer antennas [16,17].

4. CONCLUSION

A combined-type triple-wideband LTE tablet computer antenna has been proposed. The antenna can cover the LTE low band (698–960 MHz), middle band (1710–2690 MHz), and high band (3400–3800 MHz) with a small size of $10 \times 30 \times 3$ mm^3. The antenna is easily formed by combining an IFA with a coupled-fed loop antenna, with the latter enclosed by the former to achieve a compact structure. The IFA covers the LTE low band while the coupled-fed loop antenna covers the LTE middle and high bands. Operating principle of the IFA working as a low-band antenna and the coupled-fed loop antenna working as a middle/high-band antenna has been described. Experimental results of the fabricated antenna also show acceptable radiation characteristics for frequencies in the three wide operating bands for the LTE operation. The proposed combined-type antenna provides a convenient small-size antenna structure in achieving the LTE triple-wideband operation for the tablet computer application.

REFERENCES

1. L.Y. Chen and K.L. Wong, Combined-type dual-wideband antenna for 2G/3G/4G tablet device, Microwave Opt Technol Lett 56 (2014), 2799–2805.
2. K.L. Wong and C.Y. Tsai, Small-size stacked inverted-F antenna with two hybrid shorting strips for LTE/WWAN tablet device, IEEE Trans Antennas Propag 62 (2014), 3962–3969.
3. LTE frequency bands & spectrum allocations-a summary, tables of the LTE frequency band spectrum allocations for 3G & 4G LTE - TDD and FDD, Available at http://www.radio-electronics.com/.
4. Y.L. Ban, S.C. Sun, P.P. Li, J.L.W. Li, and K. Kang, Compact eight-band frequency reconfigurable antenna for LTE/WWAN tablet computer applications, IEEE Trans Antennas Propag 62 (2014), 471–474.
5. S.H. Chang and W.J. Liao, A broadband LTE/WWAN antenna design for tablet PC, IEEE Trans Antennas Propag 60 (2012), 4354–4359.
6. K.L. Wong and T.J. Wu, Small-size LTE/WWAN coupled-fed loop antenna with band-stop matching circuit for tablet computer, Microwave Opt Technol Lett 54 (2012), 1189–1193.
7. W.S. Chen and W.C. Jhang, A planar WWAN/LTE antenna for portable devices, IEEE Antennas Wireless Propag Lett 12 (2013), 19–23.
8. K.L. Wong, H.J. Jiang, and T.W. Weng, Small-size planar LTE/WWAN antenna and antenna array formed by the same for tablet computer application, Microwave Opt Technol Lett 55 (2013), 1928–1934.
9. J.H. Lu and Y.S. Wang, Internal uniplanar antenna for LTE/GSM/UMTS operation in a tablet computer, IEEE Trans Antennas Propag 61 (2013), 2841–2846.
10. J.H. Lu and F.C. Tsai, Planar internal LTE/WWAN monopole antenna for tablet computer application, IEEE Trans Antennas Propag 61 (2013), 4358–4363.
11. K.L. Wong and M.T. Chen, Small-size LTE/WWAN printed loop antenna with an inductively coupled branch strip for bandwidth enhancement in the tablet computer, IEEE Trans Antennas Propag 61 (2013), 6144–6151.
12. K.L. Wong and T.W. Weng, Coupled-fed shorted strip antenna with an inductively coupled branch strip for low-profile, small-size LTE/WWAN tablet computer antenna, Microwave Opt Technol Lett 56 (2014), 1041–1046.
13. K.L. Wong and L.Y. Chen, Coupled-fed inverted-F antenna using an inverted-F coupling feed for small-size LTE/WWAN tablet computer antenna, Microwave Opt Technol Lett 56 (2014), 1296–1302.
14. P.W. Lin and K.L. Wong, Low-profile multibranch monopole antenna with integrated matching circuit for LTE/WWAN/WLAN operation in the tablet computer, Microwave Opt Technol Lett 56 (2014), 1662–1666.
15. K.L. Wong and T.W. Weng, Very-low-profile dual-wideband tablet device antenna for LTE/WWAN operation, Microwave Opt Technol Lett 56 (2014), 1938–1942.
16. K.L. Wong and T.W. Weng, Small-size triple-wideband LTE/WWAN tablet device antenna, IEEE Antennas Wireless Propag Lett 12 (2013), 1516–1519.
17. K.L. Wong and T.W. Weng, Small-size triple-wideband LTE tablet device antenna with a wideband feed structure formed by integrated matching network, Microwave Opt Technol Lett 56 (2015), 2507–2512.
18. C.T. Lee and K.L. Wong, Planar monopole with a coupling feed and an inductive shorting strip for LTE/GSM/UMTS operation in the mobile phone, IEEE Trans Antennas Propag 58 (2010), 2479–2483.
19. C.H. Chang and K.L. Wong, Small-size printed monopole with a printed distributed inductor for penta-band WWAN mobile phone application, Microwave Opt Technol Lett 51 (2009), 2903–2908.
20. F.H. Chu and K.L. Wong, Internal coupled-fed dual-loop antenna integrated with a USB connector for WWAN/LTE mobile handset, IEEE Trans Antennas Propag 59 (2011), 4215–4221.
21. K.L. Wong, T.W. Kang, and M.F. Tu, Internal mobile phone antenna array for LTE/WWAN and LTE MIMO operations, Microwave Opt Technol Lett 53 (2011), 1569–1573.
22. K.L. Wong, W.Y. Chen, and T.W. Kang, On-board printed coupled-fed loop antenna in close proximity to the surrounding ground plane for penta-band WWAN mobile phone, IEEE Trans Antennas Propag 59 (2011), 751–757.
23. Available at http://www.ansys.com/products/hf/hfss/, ANSYS HFSS.
24. Y.W. Chi and K.L. Wong, Quarter-wavelength printed loop antenna with an internal printed matching circuit for GSM/DCS/PCS/UMTS operation in the mobile phone, IEEE Trans Antennas Propag 57 (2009), 2541–2547.
25. Y.W. Chi and K.L. Wong, Very-small-size printed loop antenna for GSM/DCS/PCS/UMTS operation in the mobile phone, Microwave Opt Technol Lett 51 (2009), 184–192.